THE JOURNAL OF PHYSICAL CHEMISTRY C

Article

Electron Induced Surface Reactions of the Organometallic Precursor Trimethyl(methylcyclopentadienyl)platinum(IV)

Joshua D. Wnuk, Justin M. Gorham, Samantha G. Rosenberg, Willem F. van Dorp, Theodore E. Madey, Cornelis W. Hagen, and D. Howard Fairbrother

J. Phys. Chem. C, **2009**, 113 (6), 2487-2496• DOI: 10.1021/jp807824c • Publication Date (Web): 21 January 2009

Electron Induced Surface Reactions of the Organometallic Precursor Trimethyl(methylcyclopentadienyl)platinum(IV)

Joshua D. Wnuk,[†] Justin M. Gorham,[†] Samantha G. Rosenberg,[†] Willem F. van Dorp,[‡,§] Theodore E. Madey,[‡,||] Cornelis W. Hagen,[§] and D. Howard Fairbrother*[,†]

Department of Chemistry, Johns Hopkins University, Baltimore, Maryland 21218, Department of Physics and Astronomy, and Laboratory for Surface Modification, Rutgers, The State University of New Jersey, Piscataway, New Jersey 08854-8019, and Delft University of Technology, Faculty of Applied Sciences, Lorentzweg 1, 2628CJ Delft, The Netherlands

Received: September 3, 2008; Revised Manuscript Received: December 7, 2008

The effect of 500 eV electrons on nanometer scale thick films of trimethyl(methylcyclopentadienyl)platinum(IV) ($MeCpPt^{IV}Me_3$), were studied in situ, under ultrahigh vacuum conditions using a combination of temperature-programmed desorption (TPD), X-ray photoelectron spectroscopy (XPS), mass spectrometry, and reflection absorption infrared spectroscopy. TPD results revealed the presence of a monolayer state, with a desorption energy >10 kJ mol^{-1} larger than the multilayer. XPS data indicate that electron beam induced decomposition of adsorbed $MeCpPt^{IV}Me_3$ produced a carbonaceous film that contained Pt atoms in an electronic state intermediate between metallic Pt and Pt(IV). In addition to Pt(IV) reduction, electron beam irradiation was also accompanied by the evolution of methane and hydrogen from the adsorbate layer and the loss of C−H groups. The rate of Pt(IV) reduction and methane production and the loss of C−H groups from the film were all proportional to the $MeCpPt^{IV}Me_3$ coverage and the incident electron flux. Rate constants for all three processes were comparable, yielding an average reaction cross section of 2.2×10^{-16} cm^2 for 500 eV electrons. Changes in the chemical composition of the adsorbate layer as a result of electron beam irradiation were consistent with a process in which one carbon atom desorbs for each $MeCpPt^{IV}Me_3$ molecule that decomposes. A comparison of the gas-phase products observed during the electron irradiation of adsorbed $MeCpPt^{IV}Me_3$ and $CpPt^{IV}Me_3$ support the idea that electron-stimulated decomposition of these platinum precursors involves by Pt−CH_3 bond cleavage.

Introduction

The applications of focused electron beams to reproducibly fabricate, modify, and etch materials at nanometer length scales are becoming increasingly prevalent.[1−6] For example, it has recently been demonstrated that electron beam induced deposition (EBID) can deposit materials with a spatial resolution below 1 nm and a mass resolution on the order of a single molecule.[7] EBID is a direct-write process where resists are not required and two- and three-dimensional nanostructures can be defined directly onto the substrate in a single step.[5,8] EBID is also used in a number of other technologically important applications, including the repair of photolithography masks,[9−11] the deposition of nanowires,[12] and high aspect ratio tips.[13] Continued improvements in the ability of direct-write, nonadiabatic processes such as EBID to design and manipulate materials at the nanoscale are needed to sustain the growth of nanotechnology and facilitate improvements in device manufacturing.

EBID is a vacuum process in which deposits are formed on a substrate by a focused electron beam in the presence of a volatile precursor.[5,6,8,14] Electron stimulated decomposition of transiently adsorbed precursor molecules are responsible for the deposition process and can in principle be initiated by either the incident primary beam or the secondary electrons generated by the interaction of the primary beam with the substrate.[12,15] Deposition and film growth occur because some of the electron stimulated reaction products are nonvolatile and remain bound to the substrate. The growth rate, composition, and structure of EBID deposits are influenced by a number of experimental parameters that include the incident beam energy, current density, and spot size as well as the chemical composition and pressure of the gas phase precursor.[5,6,8,14,16,17] Typical precursors used for the deposition of metallic nanostructures in EBID include tungsten hexacarbonyl ($W(CO)_6$,),[18−21] dimethylgold-acetylacetonate ($Me_2Au(acac)$),[22,23] and trimethyl(methylcyclopentadienyl)-platinum(IV).[1,24,25]

Despite the flexibility and processing capabilities of EBID, some significant drawbacks limit the scope of its current applications. One of the most notable disadvantages of EBID is the purity of the deposits.[26,27] During the growth of metallic nanostructures from organometallic precursors, large amounts of carbon are often codeposited along with the desired metal atoms.[25,28−30] The presence of this carbon contamination negatively impacts the electronic and optical properties of the deposited material. For example, the resistivity of Pt wires grown by EBID is often relatively high (>1 Ω cm),[28,30,31] thus limiting the application of such deposits as nanoelectrodes or nanowires.[12] Attempts to exert greater control over EBID and improve the purity of deposits have been hindered by a lack of molecular-level understanding regarding the electron stimulated reactions and chemical transformations that underpin the EBID process. This lack of knowledge is in large part a consequence of the fact that EBID is always performed in the presence of a

* Corresponding author, howardf@jhu.edu.
[†] Johns Hopkins University.
[‡] Rutgers, The State University of New Jersey.
[§] Delft University of Technology.
[||] Deceased.

10.1021/jp807824c CCC: $40.75
Published on Web 01/21/2009

constant partial pressure of the precursor.[8,14] Under these equilibrium conditions, the relatively high pressure (usually ranging from 10^{-6} Torr to a few mTorr) precludes the use of most surface analytical techniques, which are capable of monitoring changes in the chemical bonding and composition of the adsorbate layer during electron beam irradiation. The presence of a significant partial pressure associated with the EBID precursor also limits the ability of mass spectrometry to discern gas phase species evolved during the deposition process.

These limitations can, however, be circumvented by adsorbing nanoscale thin films of precursor molecules onto solid substrates at low temperatures, typically in the range 80−200 K, under ultrahigh vacuum (UHV) conditions. By variation of the gas phase exposure, the coverage of precursor molecules can be conveniently controlled. Under these conditions, the effects of electrons on the adsorbed molecules can be monitored in situ using surface analytical techniques. Indeed, this experimental approach has been successfully employed in a number of recent studies designed to examine electron mediated processes relevant to atmospheric chemistry,[32−34] astrobiology,[35] the modification of organic films[36−40] including self-assembled monolayers,[41−43] and radiation damage to biologically relevant molecules.[38,44,45] In regard to electron stimulated reactions of organometallic precursors, Yates et al. have studied the effect of low-energy (2−27 eV) electrons on the decomposition of hexafluoracetylacetonate Cu(I) vinyltrimethylsilane, a metal−organic chemical vapor deposition (MOCVD) precursor used for the deposition of copper, on the Si(7 × 7) surface at room temperature.[46] X-ray photoelectron spectroscopy (XPS) results showed that electron stimulated reactions led to the formation of Cu(0) while the threshold for decomposition was ≈4 eV, consistent with a dissociative electron attachment mechanism. Studies designed to probe electron induced reactions of organometallics adsorbed onto solid substrates under well defined experimental conditions have, however, largely focused on metal carbonyl precursors.[47−50]

In this investigation, we have studied the effect of electron beam irradiation (500 eV) on trimethyl(methylcyclopentadienyl)platinum(IV) ($MeCpPt^{IV}Me_3$) molecules adsorbed onto Au substrates under UHV conditions. $MeCpPt^{IV}Me_3$ is widely used as an organometallic precursor for Pt deposition, in not only EBID but also focused ion beam deposition, laser induced chemical processing, chemical vapor deposition, and atomic layer deposition processes.[1,24,25,52−61] In this study, we have employed TPD to probe the adsorbed state of $MeCpPt^{IV}Me_3$ on Au substrates, while XPS and reflection absorption infrared spectroscopy (RAIRS) have been used to identify changes in the chemical composition and bonding within the adsorbate layer, in situ, as a result of electron beam irradiation. Complementary analysis of the gas phase species produced during electron beam irradiation has been obtained using mass spectrometry (MS).

Experimental Section

Three separate chambers, one at Rutgers University and two at Johns Hopkins University (JHU), were used in this investigation. To probe the adsorbed state(s) of $MeCpPt^{IV}Me_3$, temperature-programmed desorption (TPD) studies were performed at Rutgers University.[62] The effect of electron beam irradiation on adsorbed $MeCpPt^{IV}Me_3$ was studied using X-ray photoelectron spectroscopy (XPS), mass spectrometry (MS), and reflection absorption infrared spectroscopy (RAIRS) at JHU.[32,33,62,63] In all of the experiments described, Au was used as the substrate. This decision was based on the ease of obtaining clean Au surfaces by Ar^+ sputtering and the comparatively high reflectivity of polished Au substrates. In TPD experiments, a polished Au(110) single crystal (1 cm diameter) was used; a 1.8 cm^2 polycrystalline Au foil was employed for XPS/MS experiments, while a polished 5.7 cm^2 polycrystalline Au substrate (Accumet) was used for RAIRS studies.

Analytical Chambers. TPD experiments were performed in an ultrahigh vacuum (UHV) chamber (base pressure ∼1×10^{-10} Torr) equipped with a UTI (model 100C) quadrupole mass spectrometer (QMS). The Au(110) substrate was mounted via Ta leads onto a Cu holder attached to a manipulator arm with capabilities for *XYZ* translation and 360° rotation. The holder design allows for liquid cooling nitrogen and resistive heating of the substrate. Prior to dosing, the sample was cleaned by Ar^+ sputtering followed by annealing in vacuum. Surface cleanliness and structure were monitored by Auger electron Spectroscopy (AES). During TPD experiments, the sample was heated by passing current through the Ta wire, producing a heating rate of 2.5 (±0.2) K/s. The substrate temperature was measured using a type K thermocouple attached to the Au substrate. Further details of the apparatus have been reported previously.[62] It should be noted that the maximum target current observed due to electron irradiation of the sample by the MS filament was 14 nA. Thus, no electron stimulated processes occurred to adsorbed $MeCpPt^{IV}Me_3$ during TPD experiments.

XPS and MS experiments were performed in an UHV chamber with a base pressure of ∼2×10^{-9} Torr. The substrate was held in a Ta sample holder, mounted at the end of a manipulator arm with capabilities for *XYZ* translation and 360° rotation. A type K thermocouple, adhered to the underside of the Ta holder, was used to measure temperature. Routine sample cleaning, which included the removal of electron beam deposited material, was performed by rastering the substrate with 4 keV Ar^+ ions for ∼30 min until XPS confirmed the substrate was >99% Au. The XPS (Physical Electronics 5400) was equipped with a Mg coated X-ray source (Physical Electronics 04-500, Mg Kα 1253.6 eV) operating at 15 kV and 300 W. Ejected photoelectrons were analyzed by a multichannel hemispherical analyzer. Unless noted, XPS experiments were conducted at a pass energy of 22.36 eV and a step size of 0.125 eV. All XPS peak positions reported in this study have been referenced to the Au($4f_{7/2}$) peak at 83.8 eV. Fits to the Pt(4f) spectral envelope were performed after the Au(4f) satellite peaks were subtracted. An example of this fitting protocol is shown in the Supporting Information (Figure 1S). On the basis of the Pt(4f) spectral envelope obtained for adsorbed $MeCpPt^{IV}Me_3$, all Pt($4f_{5/2}$/$4f_{7/2}$) transitions were fit using 60% Gaussian/40% Lorentzian peaks. Neutral gas phase products evolved during electron beam irradiation were monitored using a QMS (Stanford Research System, 0−200 amu) positioned ∼12 cm from the substrate and in a direct line-of-sight.

RAIRS experiments were performed in an UHV chamber (base pressure of ∼4×10^{-9} Torr) fitted with differentially pumped ZnSe windows. With a Cu support piece, the Au substrate was mounted onto the end of a manipulator arm capable of *XYZ* translation and 360° rotation. RAIRS spectra were recorded using a Mattson Infinity Series Fourier transform infrared spectrometer with a narrow band InSb detector (1900−4000 cm^{-1}), operating at a resolution of 4 cm^{-1}. The substrate temperature was monitored using a type K thermocouple adhered to the underside of the Cu substrate holder. The polycrystalline Au was periodically repolished to increase reflectivity.

Film Preparation. In each of the three experimental setups, the precursor $MeCpPt^{IV}Me_3$ (Aldrich), a low vapor pressure solid

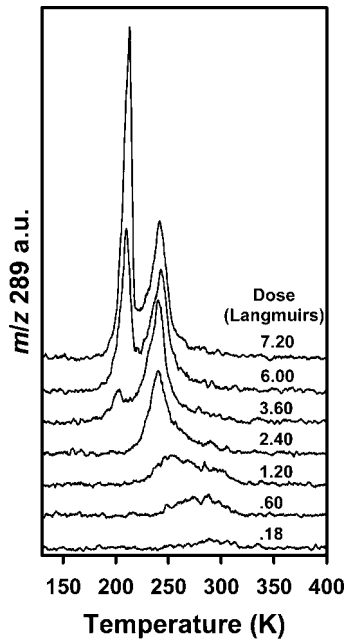

Figure 1. TPD spectra of $MeCpPt^{IV}Me_3$ adsorbed onto Au(110) measured as a function of exposure (langmuirs). In each TPD measurement the heating rate was ≈2.5 K/s.

(0.053 Torr at 23 °C),[64] was stored in an evacuated (P < 400 mTorr) glass container. The precursor was dosed into the main chamber through a UHV compatible leak valve, and the gas purity was routinely checked by QMS. In the TPD chamber the compound was directionally dosed through a gas doser (0.5 cm tube diameter) positioned approximately 2.0 cm away from the Au substrate and in a direct line-of-sight. During dosing, the local pressure enhancement of $MeCpPt^{IV}Me_3$ molecules at the surface compared to the pressure measured by the ion gauge was determined to be a factor of 60. In the XPS/MS chamber, the compound was also directionally dosed onto the substrate through a metal tube while in the RAIRS chamber the $MeCpPt^{IV}Me_3$ precursor was adsorbed by backfilling the chamber. During dosing the substrate was maintained at a temperature of ≈120 K in TPD experiments and ≈180 K in the XPS/MS and RAIRS experiments.

Determining Film Thickness/Coverage. In TPD experiments, the film coverage was determined by monitoring the desorption of the parent $MeCpPt^{IV}Me_3$ compound as a function of precursor exposure. Monolayer coverage was identified by the lowest precursor exposure required to produce a discernible multilayer peak in the TPD spectra (see Figure 1). In XPS and MS experiments, the film thickness was determined by measuring the attenuation of the XPS signal from the Au(4f) photoelectrons following $MeCpPt^{IV}Me_3$ adsorption. (This assumes an inelastic mean free path of ≈2.0 nm for Au(4f) photoelectrons.[72]) In RAIRS experiments, the film thickness was not determined quantitatively.

Electron Beam Irradiation. A commercial flood gun (Specs 15/40) was used as a source of broad electron irradiation. In the XPS/MS chamber, the substrate was positioned in a line-of-sight to the electron source at a distance of ~6 cm. RAIRS experiments were also conducted with the electron source positioned in a line-of-sight to the substrate but at a source to sample distance of ~17 cm. The flood gun produces an electron beam with a 1.0 cm full width at half-maximum at a source-to-substrate distance of 2.0 cm, ensuring a relatively uniform flux of electrons at the surface. Unless otherwise noted, the energy of the incident electrons was 500 eV. The electron energy was calculated from the sum of the electron energy generated by the flood gun and the positive bias applied to the substrate. The target current was measured to ground via a digital amp meter placed in series with the voltage source. It should be noted that no change in substrate temperature, as measured by the thermocouple, was observed during any of the electron beam irradiation experiments reported in this study.

Control experiments were also performed to investigate the stability of the deposited $MeCpPt^{IV}Me_3$ films to the X-ray irradiation generated during XPS. Results from these studies revealed that 2 h of continuous X-ray irradiation produced no measurable changes in the Pt(4f) region of a $MeCpPt^{IV}Me_3$ film deposited on polycrystalline gold at ~180 K. Surface reactions and gas phase products observed in this study can therefore be attributed solely to the effects of electrons generated by the flood gun.

Results

1. Adsorbed States of $MeCpPt^{IV}Me_3$ on Au(110). Figure 1 shows the variation in TPD spectra for the m/z = 289 peak, corresponding to the $[MeCpPtMe]^+$ ion, as a function of increasing $MeCpPt^{IV}Me_3$ exposure. To vary the $MeCpPt^{IV}Me_3$ coverage the exposure time was fixed at 100 s while the gas phase pressure during dosing was varied. For comparatively low exposures, Figure 1 shows that the desorption profile consists of a single, relatively broad peak centered at ≈290 K. As the $MeCpPt^{IV}Me_3$ coverage increases the desorption peak feature sharpens considerably and shifts down in temperature to ≈240 K. This low coverage desorption state saturates at exposures of ≈3.0 langmuirs. Using a Redhead analysis,[65] assuming first-order desorption kinetics and a pre-exponential factor of $10^{13}s^{-1}$, the desorption energy (E_{des}) of $MeCpPt^{IV}Me_3$ bound in this state decreases from 75 to 62 kJ mol^{-1} as the coverage increases.

For $MeCpPt^{IV}Me_3$ exposures >3.0 langmuirs, a sharp desorption feature appears that exhibits a peak temperature at ≈210 K. For $MeCpPt^{IV}Me_3$ exposures >3.0 langmuirs the area of this lower temperature feature increases monotonically, consistent with the formation of a multilayer state. Indeed, leading edge analysis of this state reveals good adherence to the zeroth-order desorption kinetics expected for multilayer desorption, and yields E_{des} = 53 kJ/mol.

2. Effect of Electron Beam Irradiation Probed by XPS. ***(a) Binding Energies of Pt Species.*** The XPS measurements in Figure 2a show the Pt(4f) region for a $MeCpPt^{IV}Me_3$ film deposited onto a polycrystalline Au substrate. On the basis of the Au(4f) signal attenuation the XPS spectrum in Figure 2a corresponds to a 2.52 nm thick $MeCpPt^{IV}Me_3$ film. Since the effective diameter of a $MeCpPt^{IV}Me_3$ molecule is 0.96 nm,[64] this corresponds to a coverage of between 2 and 3 monolayer equivalents. The spectral envelope in Figure 2a can be well fit with two peaks, centered at 73.8 and 77.0 eV, consistent with the spin−orbit splitting between $Pt(4f_{7/2})$ and $Pt(4f_{5/2})$ transitions; the 73.8 eV peak position (solid vertical line in Figure 2) observed for the $Pt(4f_{7/2})$ transition is indicative of Pt atoms in a highly oxidized state, consistent with the formal +4 oxidation state of Pt atoms in $MeCpPt^{IV}Me_3$.[66]

The change in the Pt(4f) region of the $MeCpPt^{IV}Me_3$ film following 20 s of irradiation by 500 eV electrons at a constant target current of 20 μA is shown in Figure 2b. Compared to Figure 2a, the Pt(4f) spectral envelope has broadened and shifted to a lower binding energy. The spectral envelope in Figure 2b can be well fit by two Pt species, with $Pt(4f_{7/2})$ peak positions at 72.0 and 73.4 eV. The 73.4 eV peak corresponds closely to the value measured in Figure 2a for the parent compound,

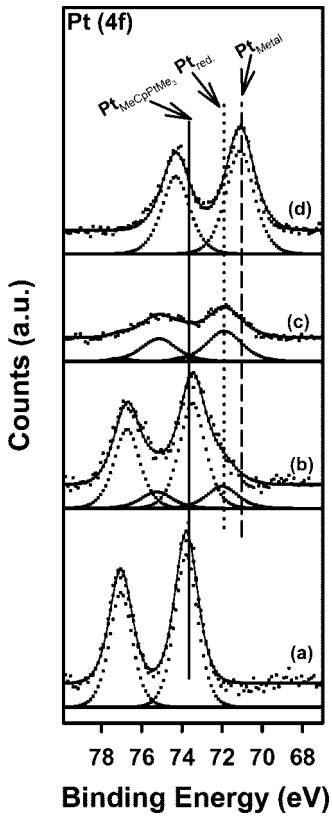

Figure 2. XPS of the Pt(4f) region measured for (a) a 2.52 nm thick $MeCpPt^{IV}Me_3$ film deposited at ≈180 K, (b) the $MeCpPt^{IV}Me_3$ film following irradiation by 500 eV electrons for 20 s at a target current of 20 μA, (c) the electron irradiated film annealed to room temperature, and (d) a sputter-deposited Pt film. The individual peaks used to fit the spectral envelope have been displaced for clarity, while the composite fits from the individual spectra are shown as solid lines through the raw data. More details can be found in the text.

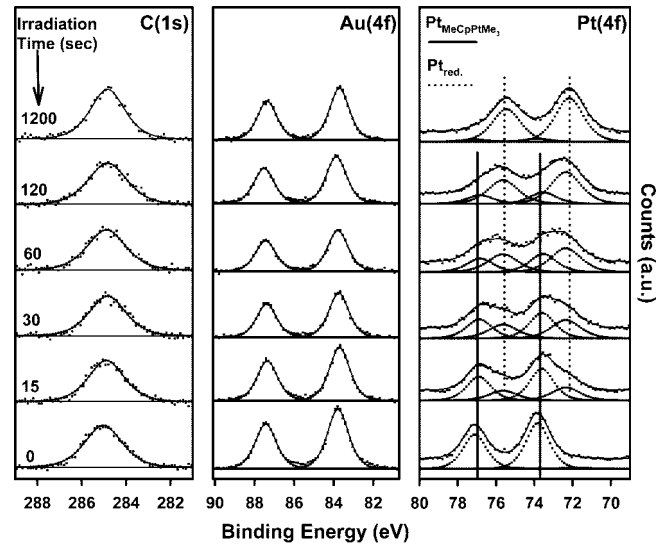

Figure 3. Evolution of the C(1s), Au(4f), and Pt(4f) XPS regions during electron irradiation (500 eV energy; 35 μA target current) of a 2.0 nm thick $MeCpPt^{IV}Me_3$ film adsorbed onto gold (∼180 K). The Pt(4f) region has been fit by two sets of Pt($4f_{5/2}$,$4f_{7/2}$) peaks, representing the parent Pt(IV) species in $MeCpPt^{IV}Me_3$ and the reduced platinum species, Pt_{red} formed by electron irradiation. The individual Pt($4f_{5/2}$, $4f_{7/2}$) peaks used to fit the spectral envelope in the Pt(4f) region have been displaced for clarity, while the composite fits from the individual spectra are shown as solid lines through the data.

although its intensity has decreased compared to Figure 2a. The peak at 72.0 eV (dotted vertical line in Figure 2) is assigned to the reduced Pt species (Pt_{red}) formed by electron irradiation of the $MeCpPt^{IV}Me_3$ film.

When the electron irradiated adsorbate layer shown in Figure 2b was annealed to room temperature, the Pt(4f) peaks associated with the parent compound disappear (cf. Figure 2c and Figure 2b). However, there is no change in the surface coverage of the Pt species formed by electron irradiation. Thus, thermal decomposition or dissociative adsorption of the $MeCpPt^{IV}Me_3$ does not contribute to the surface chemistry observed in this study. This assertion is also supported by separate AES measurements which revealed that no carbon or platinum were detected on the Au surface following $MeCpPt^{IV}Me_3$ TPD experiments.

Figure 2d shows the Pt(4f) XPS region of a sputter deposited Pt film with a thickness comparable to the $MeCpPt^{IV}Me_3$ films studied in the present investigation. This Pt(4f) spectral envelope can be well fit by two peaks centered at 71.1 and 74.3 eV, consistent with the Pt($4f_{7/2}$) and Pt($4f_{5/2}$) transitions reported for metallic Pt.[67] A comparison of panels a, c, and d of Figure 2 indicates that the Pt($4f_{7/2}$) peak position associated with the reduced Pt species formed by electron irradiation of adsorbed $MeCpPt^{IV}Me_3$ (72.0 eV) is 1.8 eV less than the value measured in Figure 2a for the (Pt(IV)) parent species (73.8 eV) but 0.9 eV greater than that observed for metallic Pt (71.1 eV).

(b) Influence of Electron Irradiation on the Chemical Composition of the Adsorbate Layer. The changes in chemical composition of a $MeCpPt^{IV}Me_3$ film as a function of electron irradiation time are shown in Figure 3. Prior to electron irradiation (irradiation time = 0 s), the Pt(4f) region can be well fit by one set of Pt($4f_{5/2}$, $4f_{7/2}$) peaks associated with the parent $MeCpPt^{IV}Me_3$ compound. After 15 s of irradiation, the Pt(4f) region broadens to lower binding energies, similar to the data shown in Figure 2b. The resultant Pt(4f) spectral envelope can be well fit by a combination of parent $MeCpPt^{IV}Me_3$ molecules and the reduced Pt species formed by electron beam irradiation (Pt_{red}). Upon further irradiation, deconvolution of the Pt(4f) region revealed that the spectral intensity associated with the parent $MeCpPt^{IV}Me_3$ species continues to decrease, while there is a corresponding increase in the surface coverage of the Pt_{red} species produced by electron irradiation. After 1200 s, reduction of the parent Pt compound is essentially complete; longer irradiation times did not produce any additional changes in the surface composition of the adlayer. Despite the visible change in the shape of the Pt(4f) XPS region during electron irradiation, the integrated area of the Pt(4f) spectral envelope remains essentially unchanged (<4%). Figure 3 also shows that although there are considerable changes in the Pt(4f) region, the C(1s) and Au(4f) spectral envelopes are largely unaffected by electron irradiation. XPS experiments also revealed that the chemical composition of the film formed by electron irradiation at ≈180 K (as measured by the C(1s) and Pt(4f) regions) was unchanged when the substrate was annealed to room temperature.

(c) Pt Reduction Kinetics. The kinetics of Pt(IV) reduction, as measured by XPS analysis of the Pt(4f) region during electron irradiation, is shown in Figure 4. In this analysis, the Pt(4f) peak areas of both the parent $MeCpPt^{IV}Me_3$ species and the reduced Pt species formed by electron irradiation have been normalized to the integrated Pt(4f) peak area measured prior to electron beam irradiation ($Pt_{(MeCpPt^{IV}Me_3)t=0}$). The normalized Pt(4f) peak area of the parent $MeCpPt^{IV}Me_3$ species have been plotted as a function of electron beam irradiation time for varying target currents. Fits to the data (shown as solid lines in Figure 4) indicate a pseudo-first-order kinetic process, whose rate constant increases with increasing target current. The inset

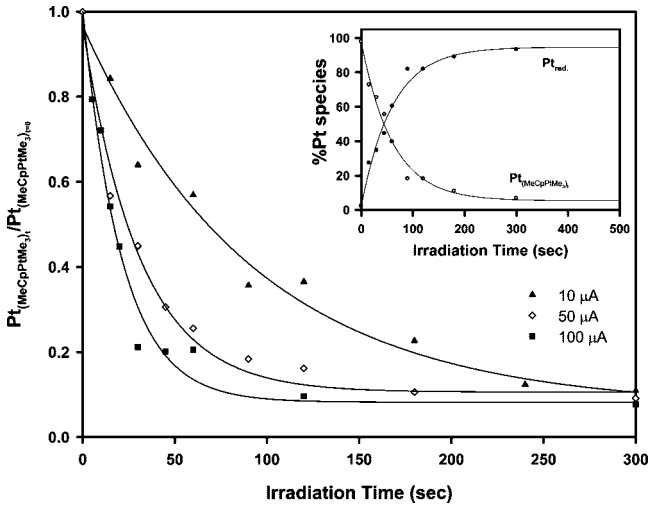

Figure 4. Variation in the normalized $MeCpPt^{IV}Me_3$ Pt(4f) XPS peak area as a function of electron irradiation time for varying target currents (10, 50, and 100 μA). (Inset) Loss and growth curves for the $MeCpPt^{IV}Me_3$ (open circles) and Pt_{red} (filled circles) species, respectively, shown as a function of electron irradiation time (500 eV, 35 μA target current). In the inset XPS peak areas are shown as a percentage of the initial Pt(4f) area before irradiation.

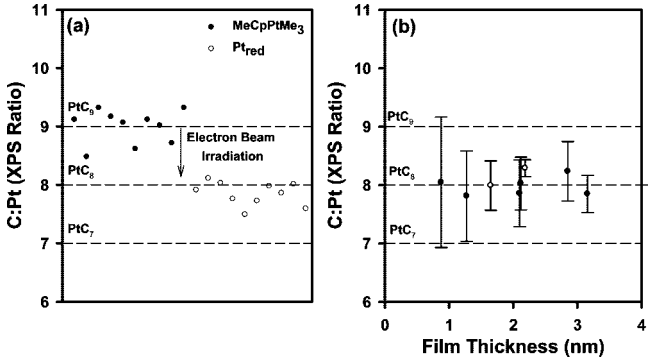

Figure 5. Influence of electron irradiation on the chemical composition of the adsorbate layer determined by XPS analysis of the Pt(4f) and C(1s) regions: (a) C:Pt ratio measured for a 3.16 nm $MeCpPt^{IV}Me_3$ film before (solid circles) and after (open circles) electron beam irradiation; (b) influence of $MeCpPt^{IV}Me_3$ film thickness on the change in C:Pt ratio following electron beam irradiation. In (b) open and closed circles represent experiments performed with 500 and 200 eV electrons, respectively. In both (a) and (b) dashed horizontal lines are shown to indicate the C:Pt ratio expected for films with a stochiometry of PtC_9, PtC_8, and PtC_7. In both (a) and (b) a pass energy of 89.5 eV was used to enhance the signal-to-noise in the C(1s) and Pt(4f) regions.

in Figure 4 illustrates that the growth of the reduced Pt species (Pt_{red}) formed by electron beam irradiation also exhibits first-order kinetics and mirrors the loss of parent Pt compound.

(d) Stoichiometry of Pt-Containing Films Formed by Electron Irradiation. Figure 5 details the systematic and reproducible change in the C:Pt ratio observed upon electron beam irradiation of adsorbed $MeCpPt^{IV}Me_3$ films. In Figure 5a, the C(1s) and Pt(4f) XPS regions of a $MeCpPt^{IV}Me_3$ film (3.16 nm average thickness) were measured repetitively over the course of 90 min of X-ray exposure. Figure 5a shows that over this period of time the C:Pt ratio (shown as solid black circles) remained constant, within experimental error. On the basis of the known stoichiometry of the parent compound, this C:Pt ratio is set to 9.0. The adsorbed $MeCpPt^{IV}Me_3$ film was then irradiated by 200 eV electrons for 27 min at a target current of 20.6 μA (shown the downward vertical arrow in Figure 5a). On the basis of the results shown in Figures 2 and 3, this electron dose was

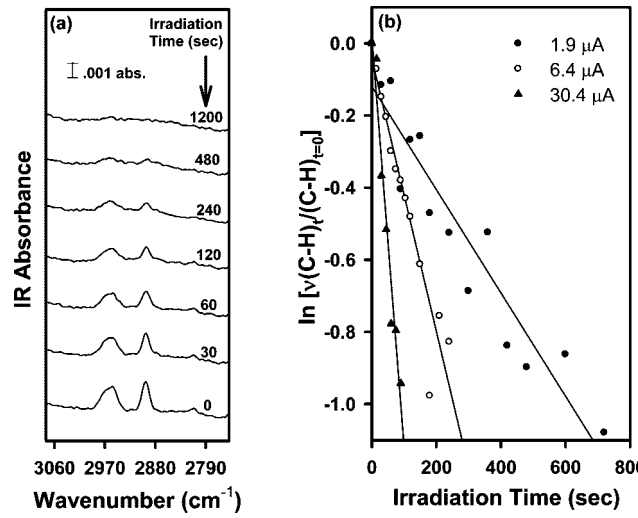

Figure 6. (a) RAIR spectra showing the effect of electron irradiation on the C−H stretching modes of $MeCpPt^{IV}Me_3$ adsorbed onto Au (~180 K). In this experiment the film was deposited following a $MeCpPt^{IV}Me_3$ exposure of 1×10^{-6} Torr for 20 min. Each spectra has been ratioed to a RAIRS spectra of the polycrystalline gold mirror prior to $MeCpPt^{IV}Me_3$ adsorption. No new IR peaks were observed during electron beam irradiation. (b) Natural logarithm of the ν(CH) IR absorbance at 2900 cm^{-1} $(C-H)_t$, normalized to the initial value prior to electron beam irradiation ($(C-H)_{t=0}$), plotted as a function of irradiation time at varying target currents. Solid lines represent fits calculated on the basis of a first-order kinetic process.

more than sufficient to decompose all of the nascent $MeCpPt^{IV}Me_3$ molecules. The C(1s) and Pt(4f) XPS regions of the Pt-containing film formed by electron irradiation were then analyzed repetitively by XPS over the course of 90 min (data shown as open circles). Analysis of Figure 5a reveals that the C:Pt ratio in the electron irradiated film had decreased from 9.0 to 7.85.

Figure 5b illustrates the fractional decrease in the C:Pt ratio observed upon electron irradiation of several $MeCpPt^{IV}Me_3$ films, measured as a function of film thicknesses. In these experiments both 500 and 200 eV electrons were used. In each experiment, the electron dose was sufficient to decompose all of the parent $MeCpPt^{IV}Me_3$ molecules. Figure 5b clearly shows that upon electron beam irradiation a reproducible change in the Pt:C ratio is observed, producing a film with $\approx PtC_8$ stoichiometry regardless of the initial $MeCpPt^{IV}Me_3$ thickness. It should be noted that in a limited set of experiments carried out at higher base pressures, nonsystematic increases in the C:Pt ratio were observed as a result of electron beam irradiation, presumably from adsorption of residual hydrocarbon species present in the vacuum chamber.

3. Effect of Electron Irradiation Probed by RAIRS: Spectroscopic and Kinetic Analysis. In Figure 6a, RAIRS data show the loss of absorbance in the ν(C−H) stretching region as a result of electron beam irradiation (500 eV energy; 25 μA target current). Prior to irradiation, the RAIRS spectrum is dominated by two ν(C−H) spectral features at 2960 and at 2900 cm^{-1} that can be assigned to the C−H stretching modes associated with the $Pt-CH_3$ and $Cp-CH_3$ groups in $MeCpPt^{IV}Me_3$.[68,69] The smaller peak observed at 2810 cm^{-1} is due to a Fermi resonance between $Pt(CH_3)_3$ modes.[68,69] Once the film is exposed to 500 eV electrons, the RAIRS peaks associated with $MeCpPt^{IV}Me_3$ decrease systematically as the electron dose increases. In Figure 6b, the natural logarithm of the IR absorbance at 2900 cm^{-1} (normalized to the absorbance measured for the $MeCpPt^{IV}Me_3$ film prior to irradiation,

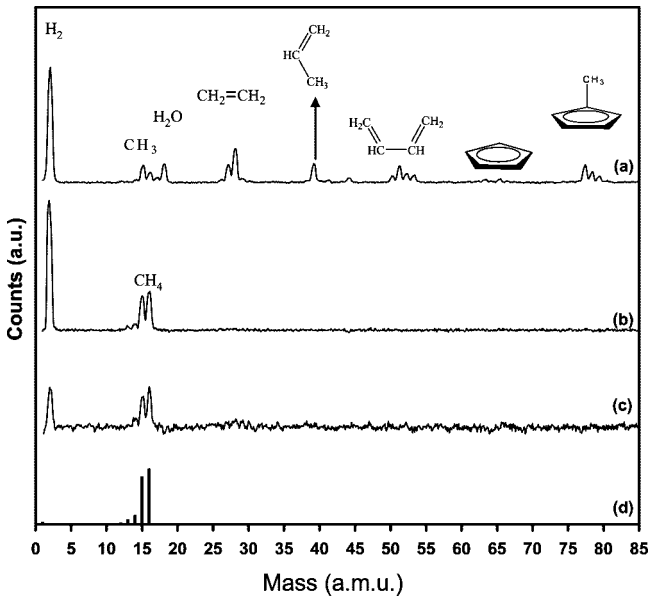

Figure 7. Mass spectrum (0−85 amu) from (a) gas phase MeCpPt^{IV}Me$_3$ and observed during the electron irradiation of (b) MeCpPt^{IV}Me$_3$ and (c) CpPt^{IV}Me$_3$ films adsorbed onto Au at ∼180 K. (d) Reference mass spectrum of CH_4(g).

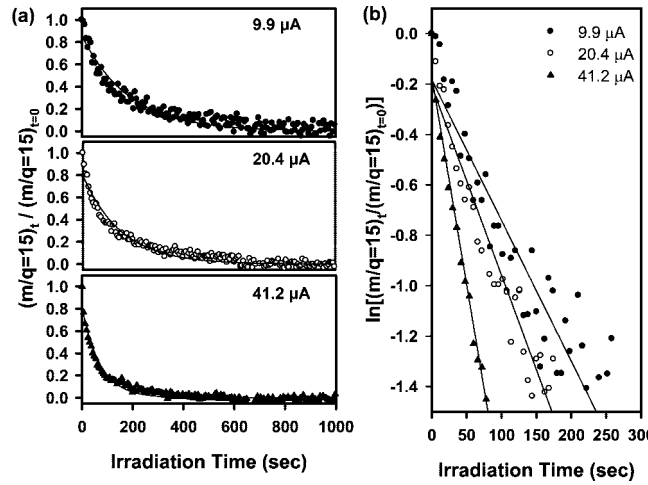

Figure 8. (a) Electron stimulated desorption kinetics of methane (measured at $m/z = 15$) as a function of electron irradiation time for varying target currents (9.9 μA, filled circles; 20.4 μA, open circles; 41.2 μA, filled triangles). (b) Natural logarithm of the normalized MS signal at $m/z = 15$ as a function of irradiation time at varying target currents. Solid lines in (a) and (b) represent fits calculated on the basis of a first-order kinetic process.

$(C-H)_{t=0}$) is plotted as a function of electron irradiation time for varying target currents. The correlation between the experimental data and the linear fits indicates that initial loss of C−H groups from the film follows first-order kinetics, with a rate constant that increases with increasing target current.

4. Effect of Electron Irradiation Probed by Mass Spectrometry. ***(a) Identification of gas phase Products.*** The mass spectrum in Figure 7 provides a comparison of the different volatile species produced when gas phase and surface-bound MeCpPt^{IV}Me$_3$ and CpPt^{IV}Me$_3$ (a Pt precursor analogous to MeCpPt(IV)Me$_3$ with the notable absence of a methyl group attached to the cyclopentadienyl ring) are exposed to electrons. In the gas phase (Figure 7a), dissociation of MeCpPt^{IV}Me$_3$ by ≈70 eV electrons yields a variety of fragments, including those associated with the methyl cyclopentadienyl ring ($m/z = 77-80$) and the methyl groups attached directly to the central Pt atom ($m/z = 15$).[70] In contrast, irradiation of adsorbed MeCpPt^{IV}Me$_3$ (Figure 7b) by 500 eV electrons produces a much simpler distribution of lower weight molecular fragments, with dominant peaks at $m/z = 2$, 15, and 16. A similar mass spectrum was observed when adsorbed CpPt^{IV}Me$_3$ was exposed to 500 eV electrons (Figure 7c). The $m/z = 15$:16 ratios observed in spectra b and c of Figure 7 are consistent with the formation of methane as the only C-containing volatile species (compare spectra b and c of Figure 7 with the reference spectrum for methane shown in Figure 7d). Thus, electron irradiation of adsorbed MeCpPt^{IV}Me$_3$ or CpPt^{IV}Me$_3$ produces hydrogen and methane as the only volatile products. It should be noted that methane and hydrogen were also the only gas phase products detected when ≈70 eV electrons were used to irradiate a MeCpPt^{IV}Me$_3$ adsorbate layer, the same electron energy used by the MS ionizer to dissociate the gas phase MeCpPt^{IV}Me$_3$ molecules in Figure 7a.

(b) Kinetics of Methane Formation. Figure 8a shows the variation in the methane MS signal (monitored at $m/z = 15$) observed during electron irradiation of adsorbed MeCpPt^{IV}Me$_3$, measured as a function of electron irradiation time for various target currents. It should be noted that $m/z = 15$ rather than $m/z = 16$ was used to measure the methane partial pressure due to the lack of any interference at $m/z = 15$ from water fragmentation in the ionizer of the mass spectrometer. In Figure 8b the natural logarithm of the normalized MS signal at $m/z = 15$ has been plotted as a function of irradiation time at varying target currents. The solid lines in Figure 8 represent fits calculated on the basis of a first-order kinetic process. The reasonable correlation between the experimental data and the solid line is consistent with the idea that methane production exhibits first-order kinetics, with a rate constant that increases with increasing target current.

A comparable analysis of the hydrogen signal observed during electron irradiation was complicated by the fact that the flood gun also acts as a source of hydrogen. This is shown explicitly in a control study (Figure 2S in Supporting Information). In this experiment a cooled Au substrate was exposed to MeCpPt^{IV}Me$_3$, subsequently cleaned of adsorbates by sputtering with Ar^+ ions (4 keV), and then irradiated by 500 eV electrons. Figure 2S shows the onset of hydrogen evolution with electron beam exposure despite the absence of any adsorbed MeCpPt^{IV}Me$_3$. To confirm that a contribution to the hydrogen signal could be ascribed to electron beam irradiation of adsorbed MeCpPt^{IV}Me$_3$, we verified that the hydrogen (and methane) MS signals both increased systematically with increasing MeCpPt^{IV}Me$_3$ film thickness.

Discussion

The discussion is organized as follows: first, the adsorption of MeCpPt^{IV}Me$_3$ onto Au as a function of surface coverage is described in the absence electron irradiation. The influence of electron irradiation on surface-bound MeCpPt^{IV}Me$_3$ is then discussed in terms of (a) the chemical reactions and resultant changes in surface chemistry that accompany electron irradiation and (b) the electron stimulated reaction kinetics and reaction cross sections. The significance and implications of the results obtained in this investigation as they pertain to EBID processes are also discussed.

Figure 1 shows that the interaction of MeCpPt^{IV}Me$_3$ with the Au substrate leads to a distinct monolayer state that is more strongly bound compared to the multilayer state observed at higher MeCpPt^{IV}Me$_3$ exposures. This energetically favorable

interaction between substrate and adsorbate is responsible for the fact that the monolayer state reaches saturation before the multilayer state is populated. Within the monolayer state, the decrease in peak desorption temperature as a function of increasing coverage for $MeCpPt^{IV}Me_3$ molecules is consistent with either the presence of preferential binding sites on the surface (e.g., at step edges or defects) or lateral interactions between the comparatively bulky $MeCpPt^{IV}Me_3$ adsorbates.[71] The TPD data presented in Figure 1 highlight the fact that favorable adsorbate−substrate interactions can exist for EBID precursors, yielding larger desorption energies (E_{des}) than would have been predicted based on the sublimation energy of the bulk material. Such phenomena must be accounted for in modeling EBID process.

Surface Reactions Induced by Electron Irradiation. XPS analysis indicates that the parent Pt(IV) forms a more reduced Pt species under the influence of electron irradiation and that for sufficiently prolonged electron doses all of the parent Pt(IV) atoms are reduced. The Pt species formed by electron irradiation also remain adsorbed at room temperature while the parent $MeCpPt^{IV}Me_3$ molecules desorb (Figures 1 and 2c). The fact that the coverage of Pt atoms stays constant during electron irradiation and the absence of any volatile fragments associated with the parent compound (see Figure 7) both support the idea that electron stimulated desorption of $MeCpPt^{IV}Me_3$ does not occur.

XPS results also showed that when the PtC_x adlayer formed by electron irradiation is heated from ≈180 K to room temperature, the coverage of carbon and platinum atoms remains constant. Under UHV conditions, any carbon containing molecules, including $MeCpPt^{IV}Me_3$, would be expected to desorb below room temperature. Consequently, the presence of adsorbed carbon atoms that are stable with respect to desorption at room temperature supports the idea that electron irradiation produces an amorphous carbon film. The Pt atoms produced by electron beam irradiation are embedded in this carbonaceous matrix (PtC_x film) and this is the reason that their electronic state is intermediate between Pt(IV) and metallic Pt (compare spectra b−d of Figure 2).

The observation of methane desorbing during electron beam irradiation demonstrates that carbon atoms are removed from the adsorbate layer as a result of electron stimulated reactions. Since there is no corresponding change in the surface coverage of Pt atoms, the C/Pt ratio should decrease as a result of electron irradiation. This hypothesis is supported by Figure 5, which illustrates that the C/Pt ratio always decreases to ≈8/9 of its nascent value after electron irradiation. Since the parent $MeCpPt^{IV}Me_3$ compound contains nine carbon atoms, this quantized change in chemical composition indicates that the overall electron stimulated reaction can be expressed as

$$MeCpPt^{IV}Me_3(ads) + e^- \rightarrow PtC_8(ads) \quad (I)$$

The formation of methane could involve electron stimulated cleavage of either a $Pt-CH_3$ bond within the parent compound, analogous to the postulated thermal and photolytic reactions of methyl Pt precursors,[53] or the $C-CH_3$ bond within the methylcyclopentadienyl ring. To elucidate which bond-breaking process is operative, we monitored the gas phase products formed when adsorbed trimethylcyclopentadienylplatinum(IV), $CpPt^{IV}Me_3$(ads), was irradiated by 500 eV electrons. Results from these studies (shown in Figure 7c) show that methane gas is still evolved, providing strong support for the idea that methane is formed by $Pt-CH_3$ and not $C-CH_3$ bond cleavage.

SCHEME 1: electron induced Reactions of Adsorbed $MeCpPt^{IV}Me_3$

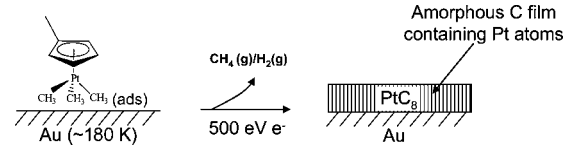

We hypothesize that the methyl radical formed in the $Pt-CH_3$ bond breaking step forms methane via intramolecular H atom abstraction. An intermolecular reaction pathway is less likely due to the lack of any ethane formation (which would be an indication of methyl radical coupling) and the fact that the methane yield increases linearly with the $MeCpPt^{IV}Me_3$ surface coverage (data not shown). Despite the ejection of methane, it should be emphasized that the majority of the carbon atoms initially associated with $MeCpPt^{IV}Me_3$ become incorporated into the Pt-containing amorphous carbon film that forms as a result of electron irradiation.

In summary, our results indicate that electron stimulated reactions of adsorbed $MeCpPt^{IV}Me_3$ produce reduced platinum atoms that become embedded in an amorphous carbon matrix. Electron induced reactions are also responsible for hydrogen and methane desorption. The overall surface reactions can be expressed as

$$MeCpPt^{IV}Me_3(ads) + e^- \rightarrow PtC_8(ads) + H_2(g)\uparrow + CH_4(g)\uparrow \quad (II)$$

In regard to EBID processes that utilize organometallic precursors, such as $MeCpPt^{IV}Me_3$, our results suggest that electron stimulated reactions involve $M-CH_3$ bond cleavage. Furthermore, it appears that the carbon atom involved in this bond breaking step "escapes" from the adsorbate layer in the form of methane while the other carbon atoms become trapped in an amorphous carbon matrix. As for the design of new precursor molecules that limit the extent of carbon deposition, our studies highlight the need for new volatile organometallic compounds with fewer carbon atoms, ideally incorporating only a single $M-CH_3$ group. It should be noted that in previous EBID studies, where the electron fluences are orders of magnitude higher than those used in the present study, the extent of carbon incorporation in deposits grown from $MeCpPtMe_3$ precursors can be reduced compared to the levels observed in the present study.[28] One possible interpretation of this difference is that under the influence of higher electron fluences multiple $M-CH_3$ bond breaking events become competitive with amorphous carbon film formation.

Kinetics of Electron Induced Processes. In addition to providing insight into the surface reactions mediated by electron irradiation, surface analytical techniques can also provide information on the reaction kinetics by monitoring the time dependence of the various surface processes. This includes the reduction of Pt(IV) atoms, the loss of C−H bonds, and the formation of methane. In our experimental setup, (a) the surface is irradiated by an electron beam whose intensity is relatively uniform across the surface, (b) the film thicknesses are on the same scale as the inelastic mean free path of the incident electrons (this is necessary to ensure a relatively uniform electron flux within the adsorbate layer), and (c) there is no electron stimulated desorption of the parent compound. As a result, the reaction rate (k) should be proportional to the concentration (surface coverage) of adsorbed parent molecules and the decrease in concentration of the parent molecule should

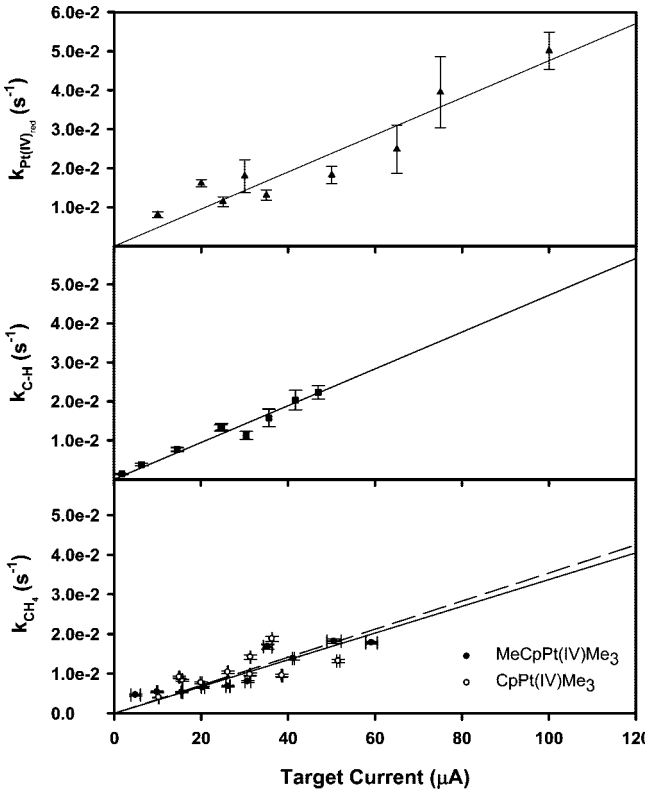

Figure 9. Variation in the pseudo-first-order rate constants for the various electron stimulated processes initiated by 500 eV electrons: Pt(IV) reduction ($k_{Pt(IV)red}$, triangles); the loss of C−H groups (k_{C-H}, squares); methane production (k_{CH_4} (solid circles, $MeCpPt^{IV}Me_3$; open circles, $CpPt^{IV}Me_3$)).

TABLE 1: Reaction Cross Sections Measured for the Various electron stimulated Processes Initiated by 500 eV Electrons, Pt(IV) Reduction ($\sigma_{Pt(IV)red}$), Loss of C−H Groups (σ_{C-H}), and Methane Production (σ_{CH_4})[a]

	σ (cm^2)
$\sigma_{Pt(IV)red}$	1.37×10^{-16}
σ_{C-H}	4.32×10^{-16}
σ_{CH_4} ($MeCpPt^{IV}Me_3$)	9.75×10^{-17}
σ_{CH_4} ($CpPt^{IV}Me_3$)	1.02×10^{-16}

[a] For methane production, the average cross sections are shown for both $MeCpPt^{IV}Me_3$ and $CpPt^{IV}Me_3$.

follow pseudo-first-order kinetics under the influence of a constant electron flux (target current).[41] The reaction cross section (σ) can be calculated from the pseudo-first-order rate constant, provided that both the incident electron flux and irradiated area are known.

Figure 4 demonstrates that the kinetics of Pt(IV) reduction can be described by a first-order loss process with respect to the coverage of $MeCpPt^{IV}Me_3$ molecules. It should be noted that the fact that the surface coverage of parent Pt(IV) atoms does not decrease to exactly 0% is a consequence of the fact that the Pt(4f) spectral envelope associated with the Pt species produced by electron beam irradiation could not be perfectly fit by a single set of Pt($4f_{7/2}$/$4f_{5/2}$) transitions. This broadening of the Pt(4f) spectral envelope is probably a result of the heterogeneity in the local environment experienced by Pt atoms in the amorphous carbon matrix. As a result, the Pt(4f) spectral envelope always appeared to contain a small contribution from the parent compound, even when PtC_x films were annealed to temperatures where any adsorbed $MeCpPt^{IV}Me_3$ would have desorbed. Since this inaccuracy in the spectral deconvolution is small (<10% of the integrated Pt(4f) intensity), we have ignored it in our kinetic analysis of the Pt reduction process.

Analysis of Figure 9 demonstrates that the pseudo-first-order rate constants for Pt(IV) reduction ($k_{Pt\text{-}red}$) also vary linearly with the incident electron flux. Thus, the overall kinetics of Pt(IV) reduction can be described by the following equation, where $[MeCpPt^{IV}Me_3](ads)$ represents the coverage of precursor molecules in units of molecules/cm^2;

$$\frac{d[Pt_{red}]}{dt} = -\frac{d[MeCpPt^{IV}Me_3]}{dt} = k_{Pt\text{-}red}[MeCpPt^{IV}Me_3](ads) \quad \text{(III)}$$

The RAIRS data also show that the initial loss of C−H groups can be reasonably well described by a first-order kinetic process whose rate constant (k_{C-H}) varies linearly with the target current (see Figures 6b and 9). The kinetic analysis of the RAIRS data was restricted to the initial stages of the reaction due to the fact that the film thicknesses in these experiments were certainly larger than the inelastic mean free path of the incident 500 eV electrons. In such thicker films, a slow "tailing" is expected to be observed in the loss kinetics and indeed this was routinely observed experimentally. In contrast, $MeCpPt^{IV}Me_3$ film thicknesses in both XPS and MS measurements were typically on the order of 1−3 nm, comparable to the inelastic mean free path of 500 eV electrons (≈2 nm).[72]

The rate of methane production (k_{CH_4}) during electron irradiation of adsorbed $MeCpPt^{IV}Me_3$ and $CpPt^{IV}Me_3$ could also be described by first-order kinetics with a rate constant (k_{CH_4}) that varied linearly with the target current (see Figures 8 and 9). As noted in the results section, although hydrogen was observed as the other gas phase product formed during electron beam irradiation, a detailed kinetic analysis was precluded by the fact that hydrogen was also evolved from the electron filament (see Supporting Information, Figure 2). However, since the time scale over which hydrogen and methane production are observed was comparable, we believe that the rate of electron stimulated hydrogen production is comparable to k_{CH_4}.

Figure 9 shows the variation in the pseudo-first-order rate constants ($k_{Pt(IV)red}$, k_{C-H}, and k_{CH_4}) for each surface process, as a function of the target current. From this information the corresponding reaction cross sections (σ) can be determined using the following equation

$$\sigma_a = \frac{k_a}{I_{target}} \times \text{sample area } (cm^2) \quad \text{(IV)}$$
$$a = Pt(IV)_{red}, C-H, CH_4$$

where I_{target} is the target current in units of electrons/s. The gradients in Figure 9 were used to calculate the average k_a/I_{target} values for each surface process. Results from this analysis, shown in Table 1, reveal that the reaction cross sections measured for each of the various processes (reduction of Pt(IV), loss of C−H bonds, desorption of methane) are comparable. This is striking, given that these measurements reflect rate constants measured using two separate UHV chambers and three different analytical techniques. Thus, the overall reaction kinetics can be described by the following expression

$$-\frac{d[MeCpPt^{IV}Me_3]}{dt} = \frac{d[PtC_x]}{dt} = -\frac{d[CH_4]}{dt} = -\frac{d[C-H]}{dt} = \sigma I_{target}[MeCpPt^{IV}Me_3](ads) \quad \text{(V)}$$

On the basis of these measurements, we calculate an average reaction cross section, $\sigma_{rx}(500\text{ eV}) = 2.2 \times 10^{-16}$

cm^2 for the electron stimulated reactions of $MeCpPt^{IV}Me_3$, assuming equal weighting from XPS, RAIRS, and MS measurements. A similar value (1.0×10^{-16} cm^2) was also measured for σ_{CH_4} during e-beam irradiation of $CpPt^{IV}Me_3$. Although we are unable to measure the kinetics of hydrogen evolution, our results suggest that the reaction cross section for H_2 production (σ_{H_2}) is of a similar magnitude to σ_{CH_4} for both $MeCpPt^{IV}Me_3$ and $CpPt^{IV}Me_3$.

Our kinetic analysis also implies that the rate-determining step in the reduction of Pt(IV) species, the loss of C−H groups, and the formation of methane involves a single electron event, consistent with the idea that the rate-determining step involves electron stimulated $Pt-CH_3$ bond cleavage accompanied by the formation of methane. This hypothesis is also supported by the similar reaction cross sections measured for $MeCpPt^{IV}Me_3$ and $CpPt^{IV}Me_3$.

Conclusions

Trimethyl(methylcyclopentadienyl)platinum(IV) ($MeCpPt^{IV}Me_3$) adsorbed on Au substrates at 180 K undergoes electron stimulated decomposition mediated by $Pt-CH_3$ bond cleavage. Decomposition of the parent compound results in the reduction of platinum atoms and the evolution of gas phase methane and hydrogen. Platinum atoms formed by electron beam irradiation become embedded in an amorphous carbon matrix and exhibit an electronic state which is intermediate between Pt(IV) and metallic Pt. Electron beam irradiation is also responsible for a reproducible decrease in the film's C/Pt ratio, whose magnitude is consistent with the idea that electron induced decomposition of each $MeCpPt^{IV}Me_3$ molecule is accompanied by desorption of one carbon atom. The rate of Pt reduction, the loss of C−H bonds from the film, and methane production are all proportional to the $MeCpPt^{IV}Me_3$ coverage and display comparable rate constants. The average reaction cross section for adsorbed $MeCpPt^{IV}Me_3$ exposed to 500 eV electrons is calculated to be 2.2×10^{-16} cm^2. This study highlights the ability of surface analytical techniques to obtain mechanistic information that cannot be obtained in typical EBID processes. This includes providing structural requirements for new precursors that will produce EBID nanostructures with more desirable materials properties. Such information is particularly important for platinum-based nanostructures which are expected to play an important role in future nanoelectronics, due to the chemical stability, resistance to oxidation, and high thermal conductivity of platinum.

Acknowledgment. The authors acknowledge support from the National Science Foundation (# CHE-0616873). The assistance of Boris Yakshinskiy and Shimon Zalkind at Rutgers University in helping with the TPD experiments is also gratefully acknowledged.

Supporting Information Available: An example of the fitting protocol used to analyze the Pt(4f) region, the experimental protocol, and variation in *m/z* signals for a sputter-cleaned Au surface exposed to electron beam irradiation. This material is available free of charge via the Internet at http://pubs.acs.org.

References and Notes

(1) Gazzadi, G. C.; Frabboni, S. *J. Vac. Sci. Technol., B* **2005**, *23*, L1.
(2) Toth, M.; Lobo, C. J.; Knowles, W. R.; Phillips, M. R.; Postek, M. T.; Vladar, A. E. *Nano Lett.* **2007**, *7*, 525.
(3) Rack, P. D.; Fowlkes, J. D.; Randolph, S. J. *Nanotechnology* **2007**, *18*, 465602.
(4) Choi, Y. R.; Rack, P. D.; Frost, B.; Joy, D. C. *Scanning* **2007**, *29*, 171.
(5) Utke, I.; Hoffmann, P.; Melngailis, J. *J. Vac. Sci. Technol., B* **2008**, *26*, 1197.
(6) van Dorp, W. F.; Hagen, C. W. *J. Appl. Phys.* **2008**, *104*, 081301.
(7) van Dorp, W. F.; van Someren, B.; Hagen, C. W.; Kruit, P.; Crozier, P. A. *Nano Lett.* **2005**, *5*, 1303.
(8) Randolph, S. J.; Fowlkes, J. D.; Rack, P. D. *Crit. Rev. Solid State Mater. Sci.* **2006**, *31*, 55.
(9) Liang, T.; Stivers, A. Damage-free Mask Repair Using Electron Beam Induced Chemical Reactions. *Proc. SPIE* **2002**, Vol. 4688.
(10) Liang, T.; Frendberg, E.; Lieberman, B.; Stivers, A. *J. Vac. Sci. Technol., B* **2005**, *23*, 3101.
(11) Edinger, K.; Becht, H.; Bihr, J.; Boegli, V.; Budach, M.; Hofmann, T.; Koops, H. W. P.; Kuschnerus, P.; Oster, J.; Spies, P.; Weyrauch, B. *J. Vac. Sci. Technol., B* **2004**, *22*, 2902.
(12) Silvis-Cividjian, N.; Hagen, C. W.; Kruit, P.; v.d. Stam, M. A.; Groen, H. B *Appl. Phys. Lett.* **2003**, *82*, 3514.
(13) Utke, I.; Hoffmann, P.; Berger, R.; Scandella, L. *Appl. Phys. Lett.* **2002**, *80*, 4792.
(14) Silvis-Cividjian, N.; Hagen, C. W. *Adv. Imaging Electron Phys.* **2006**, *143*, 1.
(15) Smith, D. A.; Fowlkes, J. D.; Rack, P. D. *Nanotechnology* **2007**, *18*, 265308.
(16) Tanaka, M.; Shimojo, M.; Mitsuishi, K.; Furuya, K. *Appl. Phys. A: Mater. Sci. Process.* **2004**, *78*, 543.
(17) Hoffman, P.; Utke, I.; Cicoira, F. Limits of 3-D Nanostructures Fabricated by Focused Electron Beam (FEB) Induced Deposition. *Proc. SPIE* **2003**.
(18) Hoyle, P. C.; Cleaver, J. R. A.; Ahmed, H. *J. Vac. Sci. Technol., B* **1996**, *14*, 662.
(19) Koops, H. W. P.; Weiel, R.; Kern, D. P.; Baum, T. H. *J. Vac. Sci. Technol., B* **1988**, *6*, 477.
(20) Hoyle, P. C.; Ogasawara, M.; Cleaver, J. R. A.; Ahmed, H. *Appl. Phys. Lett.* **1993**, *62*, 3043.
(21) Rack, P. D.; Randolph, S.; Deng, Y.; Fowlkes, J.; Choi, Y.; Joy, D. C. *Appl. Phys. Lett.* **2003**, *82*, 2326.
(22) Graells, S.; Alcubilla, R.; Badenes, G.; Quidant, R. *Appl. Phys. Lett.* **2007**, *91*, 121112.
(23) Ketharanathan, S.; Sharma, R.; Drucker, J. *J. Vac. Sci. Technol., B* **2005**, *23*, 2403.
(24) Frabboni, S.; Gazzadi, G. C.; Felisari, L.; Spessot, A. *Appl. Phys. Lett.* **2006**, *88*, 213116.
(25) Frabboni, S.; Gazzadi, G. C.; Spessot, A. *Physica E* **2007**, *37*, 265.
(26) Cicoira, F.; Leifer, K.; Hoffmann, P.; Utke, I.; Dwir, B.; Laub, D.; Buffat, P. A.; Kapon, E.; Doppelt, P. *J. Cryst. Growth* **2004**, *265*, 619.
(27) Shimojo, M.; Takeguchi, M.; Tanaka, M.; Mitsuishi, K.; Furuya, K. *Appl. Phys. A: Mater. Sci. Process.* **2004**, *79*, 1869.
(28) Botman, A.; Hesselberth, M.; Mulders, J. J. L. *Microelectron. Eng.* **2008**, *85*, 1139.
(29) Folch, A.; Servat, J.; Esteve, J.; Tejada, J.; Seco, M. *J. Vac. Sci. Technol., B* **1996**, *14*, 2609.
(30) Botman, A.; Mulders, J. J. L.; Weemaes, R.; Mentink, S. *Nanotechnology* **2006**, *17*, 3779.
(31) Koops, H. W.; Kaya, A.; Weber, M. *J. Vac. Sci. Technol., B* **1995**, *13*, 2400.
(32) Perry, C. C.; Wolfe, G. M.; Wagner, A. J.; Torres, J.; Faradzhev, N. S.; Madey, T. E.; Fairbrother, D. H. *J. Phys. Chem. B* **2003**, *107*, 12740.
(33) Wagner, A. J.; Vecitis, C.; Fairbrother, D. H. *J. Phys. Chem. B* **2002**, *106*, 4432.
(34) Nakayama, N.; Wilson, S. C.; Stadelmann, L. E.; Lee, H.-L. D.; Cable, C. A.; Arumainayagam, C. R. *J. Phys. Chem. B* **2004**, *108*, 7950.
(35) Lafosse, A.; Bertin, M.; Domaracka, A.; Pliszka, D.; Illenberger, E.; Azria, R. *Phys. Chem. Chem. Phys.* **2006**, *8*, 5564.
(36) Swiderek, P.; Jäggle, C.; Bankmann, D.; Burean, E. *J. Phys. Chem. C* **2007**, *111*, 303.
(37) Swiderek, P. *Eur. Phys. J. D* **2005**, *35*, 355.
(38) Breton, S.-P.; Michaud, M.; Jäggle, C.; Swiderek, P.; Sanche, L. *J. Chem. Phys.* **2004**, *121*, 11240.
(39) Weeks, L. D.; Zhu, L. L.; Pellon, M.; Haines, D. R.; Arumainayagam, C. R. *J. Phys. Chem. C* **2007**, *111*, 4815.
(40) Harris, T. D.; Lee, D. H.; Blumberg, M. Q.; Arumainayagam, C. R. *J. Phys. Chem.* **1995**, *99*, 9530.
(41) Olsen, C.; Rowntree, P. A. *J. Chem. Phys.* **1998**, *108*, 3750.
(42) Wagner, A. J.; Carlo, S. R.; Vecitis, C.; Fairbrother, D. H. *Langmuir* **2002**, *18*, 1542.
(43) Heister, K.; Zharnikov, M.; Grunze, M.; Johansson, L. S. O.; Ulman, A. *Langmuir* **2001**, *17*, 8.
(44) Klyachko, D.; Gantchev, T.; Huels, M. A.; Sanche, L. *R. Soc. Chem.* **1997**, *204*, 85.
(45) Klyachko, D. V.; Huels, M. A.; Sanche, L. *Radiat. Res.* **1999**, *151*, 177.

(46) Mezhenny, S.; Lyubinetsky, I.; Choyke, W. J.; Yates, J., J.T. *J. Appl. Phys.* **1999**, *85*, 3368.
(47) Foord, J. S.; Jackman, R. B. *Surf. Sci.* **1986**, *171*, 197.
(48) Henderson, M. A.; Ramsier, R. D.; Yates, J., J.T. *Surf. Sci.* **1991**, *259*, 173.
(49) Ramsier, R. D.; Henderson, M. A.; Yates, J., J.T. *Surf. Sci.* **1991**, *257*, 9.
(50) Henderson, M. A.; Ramsier, R. D.; Yates, J., J.T. *J. Vac. Sci. Technol., A* **1991**, *9*, 1563.
(51) Ramsier, R. D.; Yates, J., J.T. *Surf. Sci.* **1993**, *289*, 39.
(52) Gopal, V.; Stach, E. A.; Radmilovic, V. R.; Mowat, I. A. *Appl. Phys. Lett.* **2004**, *85*, 49.
(53) Thurier, C.; Doppelt, P. *Coord. Chem. Rev.* **2008**, *252*, 155.
(54) Telari, K. A.; Rogers, B. R.; Fang, H.; Shen, L.; Weller, R. A.; Braski, D. N. *J. Vac. Sci. Technol., B* **2002**, *20*, 590.
(55) Dunn, K. A.; Breslin, C.; Thiel, B. L. *Microsc. Microanal.* **2006**, *12*, 1282.
(56) Tao, T.; Ro, J.; Meingailis, J.; Xue, Z.; Kaesz, H. D. *J. Vac. Sci. Technol., B* **1990**, *8*, 1826.
(57) Tao, T.; Wilkinson, W.; Meingailis, J. *J. Vac. Sci. Technol., B* **1991**, *9*, 162.
(58) DeMarco, A. J.; Meingailis, J. *J. Vac. Sci. Technol., B* **1999**, *17*, 3154.
(59) Xu, Q. Y.; Kageyama, Y.; Suzuki, T *J. Appl. Phys.* **2005**, *97*, 10K308.
(60) Aaltonen, T.; Ritala, M.; Sajavaara, T.; Keinonen, J.; Leskela, M. *Chem. Mater.* **2003**, *15*, 1924.
(61) Jiang, X.; Bent, S. F. *J. Electrochem. Soc.* **2007**, *154*, D648.
(62) Faradzhev, N. S.; Perry, C. C.; Kusmierek, D. O.; Fairbrother, D. H.; Madey, T. E. *J. Chem. Phys.* **2004**, *121*, 8547.
(63) Carlo, S. R.; Torres, J.; Fairbrother, D. H. *J. Phys. Chem. B* **2001**, *105*, 6148.
(64) Xue, Z.; Strouse, M. J.; Shuh, D. K.; Knobler, C. B.; Kaesz, H. D.; Hicks, R. F.; Williams, R. S. *J. Am. Chem. Soc.* **1989**, *111*, 8779.
(65) Redhead, P. A. *Vacuum* **1962**, *12*, 203.
(66) Sen, F.; Goekagac, G. *J. Phys. Chem. C* **2007**, *111*, 5715.
(67) Watanabe, M.; Uchida, M.; Motoo, S. *J. Electroanal. Chem.* **1987**, *229*, 395.
(68) Hall, J. R.; Smith, B. E. *Aust. J. Chem.* **1971**, *24*, 911.
(69) Parker, D. J.; Stiddard, M. H. B. *J. Chem. Soc. A* **1970**, 1040.
(70) Cahill, J. J.; Panayotov, V. G.; Cowen, K. A.; Harris, E.; Koplitz, L. V.; Birdwhistell, K.; Koplitz, B. *J. Vac. Sci. Technol, A* **2007**, *25*, 104.
(71) King, D. A. *Surf. Sci.* **1975**, *47*, 384.
(72) Tanuma, S.; Powell, C. J.; Penn, D. R. *Surf. Interface Anal.* **1991**, *17*, 927.
(73) Lo Nigro, R.; Malandrino, G.; Fiorenza, P.; Fragala, I. L. *ACS Nano* **2007**, *1*, 183.

JP807824C